Ir Film Structural Properties for TES Application

L. Ferrari Barusso, S. Tugliani, M. Fedkevych, E. Celasco, G. Gallucci, D. Grosso, P. Manfrinetti, K. Niazi, and F. Gatti

***Abstract*—Iridium films grown by pulsed laser deposition (PLD) show different critical temperatures (T_c), which can be almost twice the T_c of the bulk. This difference is related to the thickness and deposition conditions. To understand this effect, we grew different films with different configuration parameters: laser focusing, distance to the Ir target, and deposition time. We then measured the T_c and analyzed the film with structural measurements by X-ray diffraction (XRD), looking at a possible correlation with the grain size of the film itself. The work was performed to determine the film growth conditions at which it is possible to obtain predetermination of T_c with good accuracy using XRD pattern characteristics of Ir films.**

***Index Terms*—TES, XRD, iridium, superconductivity, T_c, critical temperature, PLD, X-rays astrophysics.**

I. Introduction

TRANSITION Edge Sensors (TES) for use in cryogenic detectors require accurate characterizations for the determination of operational parameters such as critical temperature Tc, resistivity ρ and the shape of superconductor-normal transitions. These depend not only on construction details, such as geometry and size, but also on micro-structural and morphological parameters, such as the microcrystalline structures of the films, their orientations, the sizes of the crystalline grains, and the stresses to which they are subjected by lattice mismatch with the substrate.In this paper we report the analysis of iridium films on silicon substrates for the fabrication of TES based cryogenic anti-coincidence detector, the Cryo-AC, [1], [2], [3], [4], [5], that will operate on the focal plane of the future X-ray space telescope ATHENA [6].

A systematic correlation between the size of crystalline domains in the iridium film and the critical temperature T_c of the film itself is highlighted.

Manuscript received 9 January 2023; revised 24 February 2023; accepted 6 March 2023. Date of publication 16 March 2023; date of current version 6 April 2023. This work was supported by the Italian Space Agency ASI under Grant 2019-27-HH.0. *(Corresponding author: L. Ferrari Barusso.)*

L. Ferrari Barusso, E. Celasco, D. Grosso, and F. Gatti are with the Università di Genova and INFN Genova, 16146 Genoa, Italy (e-mail: lorenzo.ferrari@ge.infn.it).

S. Tugliani is with the Università di Torino, 10124 Turin, Italy.

M. Fedkevych is with the Department of Physics and Astronomy, The University of Alabama, Tuscaloosa, AL 35487 USA.

G. Gallucci is with the INFN Genoa, 16146 Genoa, Italy.

P. Manfrinetti and K. Niazi are with the Università di Genova, 10124 Genova 16146, Italy.

Color versions of one or more figures in this article are available at https://doi.org/10.1109/TASC.2023.3257822.

Digital Object Identifier 10.1109/TASC.2023.3257822

II. Sample Preparation

Film samples were prepared by pulsed laser deposition (PLD) of Ir on large chips (15×15 mm^2) cut from high resistivity ($\rho >$ 10000 Ωm) intrinsic silicon wafers with orientation (100). PLD systems for Ir growth employ an Nd:YAG infrared laser at a wavelength of 1064 nm, with pulses of 10 ns and energy of 750 mJ at a repetition rate of 10 Hz. Before Ir deposition, the silicon substrates are cleaned of organic residues with various solvents and of metallic residues and oxides by the RCA process, i.e., a standard sequence of dilute water baths of NH_4OH, HF, HCl. Ir deposition takes about 30–45 min, at the end of which time the sample is brought into the chamber for gold film deposition without interrupting the vacuum. The Au film is grown on the iridium layer with evaporation by electron beam (e-Beam). At the end of deposition, the sample is extracted from the deposition systems and cut into several samples on each of which various measurements are made: (i) absolute thickness of the film with an interferometric optical profilometer, (ii) resistivity at room temperature and low temperature, (iii) critical temperature, and (iv) structural and morphological analysis. Thickness measurements are made using the edge generated by shadowing of structures placed on chips before film deposition. We measure the height difference between the silicon substrate and the top surface of the film using a Shaeffer's optical profilometer with an overall accuracy of about 5 nm.

Resistivity measurements are performed by the 4-probe Kelvin method, via 4 aluminum wires of 25 μm diameter ultrasonically welded inline in the center of the large-area film. Film resistance is measured at room temperature, in liquid helium, and at 100 mK in a He-3/He-4 dilution refrigerator (Oxford Instrument Kelvinox 25)

Structural measurements are made in the Hewlett Packard XRD system that has an X-ray beam produced with copper cathode.

The critical temperature T_c measurements have the appearance shown in Fig. 2 for two significant cases related to grA and grB sample group.

Typical XRD spectra obtained for the bare silicon substrate and for the bilayer of Ir and IrAu that we grew on the same substrates are shown in Fig. 1.

The spectra show a recognizable pattern with overlapping peaks for each material: silicon (100) has the characteristic reflection line (400) doubled due to the two X-ray energy Kα and Kβ emission lines of the copper cathode; Ir films grow with a preferred structure (111), plus sub-structures (110) and (311); Au films grow over Ir with the same crystal orientation as Ir, i.e., Au(111) over Ir(111) and Au(222) over Ir(222).

This work is licensed under a Creative Commons Attribution 4.0 License. For more information, see https://creativecommons.org/licenses/by/4.0/

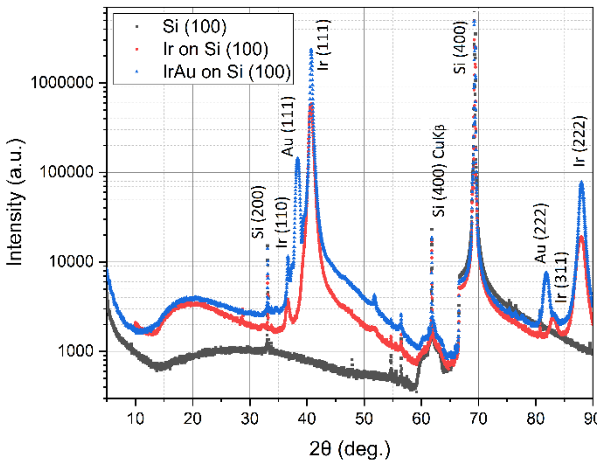

Fig. 1. Spectra have a recognizable footprint with superimposed peaks for each material. Silicon (100) presents the characteristic (400) reflection, the Ir films grow with a preferred (111) structure plus (110) and (311) substructures, and Au films grow on top following the Ir crystalline orientation.

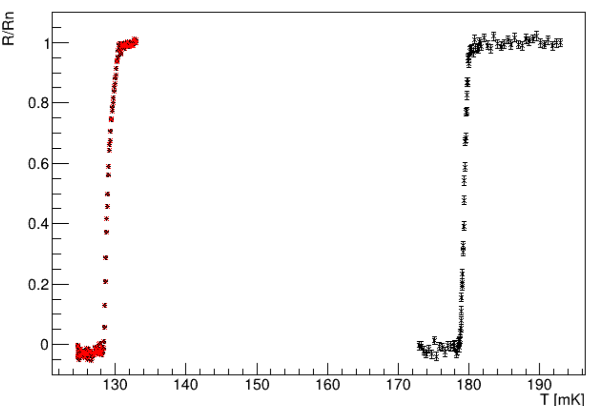

Fig. 2. The T_c can be derived from the reported measurements, which are *R/Rn* vs *T*.

III. T_c AND XRD

Over the years, we have had evidence that samples of Ir films on Silicon (100) showed quite different T_c temperatures, about 50 mK, although the growth conditions were similar. In particular, we know that the growth system experienced slight differences in deposition parameter over time, such as spot size on the Ir target and target-substrate distance. Therefore, we supposed that these differences had affected the crystal structure and film morphology. Thus, we selected two Ir samples having T_c of 130 and 180 mK, respectively, to check whether differences in the crystal structure of the two samples were also present. A preliminary analysis shows no significant difference between the patterns shown in Fig. 1. However, by performing measurements with greater statistics and precision and focusing on individual lines, as shown in Fig. 3, we observed a reproducible shift in the Ir (222) lines of the order of 0.08°. We verified that the shift was not due to instrumental causes, i.e., a rigid shift in the entire XRD pattern due to differences in orientation between samples, the Si (400) lines being perfectly overlapping.

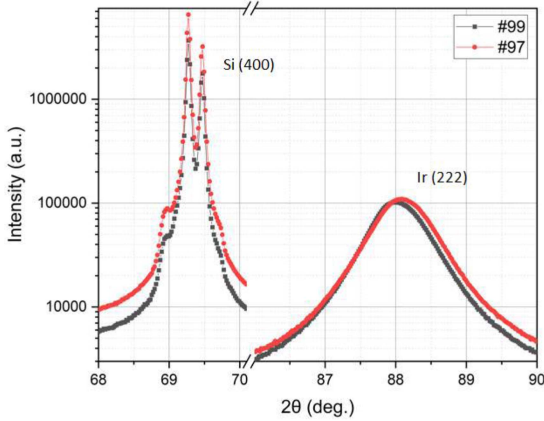

Fig. 3. Particular of the (400) Silicon peak and the (222) Ir peak for the Ir film #97 with 130 mK T_c and the Ir film #99 with 180 mK T_c. The (400) peaks are aligned while the (222) present a shift of the maximum.

TABLE I
GAUSSIAN FIT OF IR AND IRAU LINES OF EXAMINED FILMS: POSITION(MAXIMUM) θ AND FWHM β ARE LISTED. ERRORS ARE ON THE LAST DIGIT

Sample	110	111	311	222	
97 (grA)	36,687	40,777		88,070	θ
T_c 130mK	0,356	0,376		0,873	β
99 (grB)	36,654	40,749		87,994	Θ
T_c 180mK	0,346	0,322		0,835	β
106 (grA)	36,670	40,780		88,069	θ
T_c 130mK	0,592	0,509		1,274	β
107 (grA)	36,668	40,766		88,072	θ
T_c 130mK	0,528	0,447		1,075	β
108 (grA)	36,669	40,778	83,376	88,086	θ
T_c 130mK	0,377	0,380	0,602	0,963	β
111 (grB)	36,652	40,737	83,347	87,988	θ
T_c 180mK	0,330	0,322	0,886	0,858	β
112 (grB)	36,669	40,757		88,028	θ
T_c 180mK	0,338	0,304		0,790	β
113 (grA)	36,721	40,789		88,098	θ
T_c 130mK	0,478	0,411		0,956	β
114 (grB)	36,656	40,739		88,004	θ
T_c 180mK	0,335	0,329		0,840	β

We then analyzed the microscopic structure of a series of 9 bilayer samples of IrAu and looked for the same pattern that emerged from the line analysis shown in Fig. 3. To uniformly calculate the magnitude of the displacement of all examined films, we have fitted with a Gaussian function to measure the line positions (maximum of the fit function θ) and the Full Width at Half Maximum (FWHM) β of each visible iridium-related line. The results are summarized in Table I.

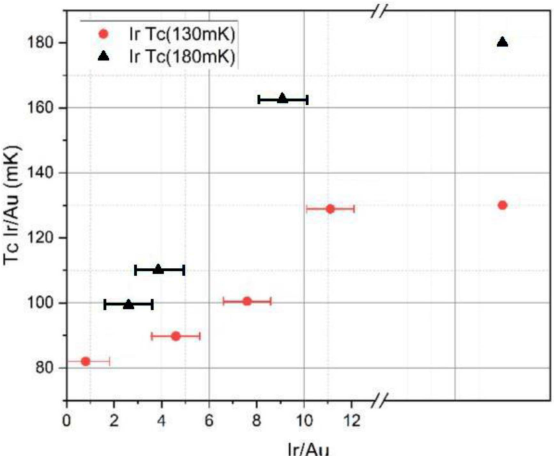

Fig. 4. Critical temperature of IrAu bilayer as function of the Iridium and Gold thickness ratio. The two Ir critical temperature are highlighted.

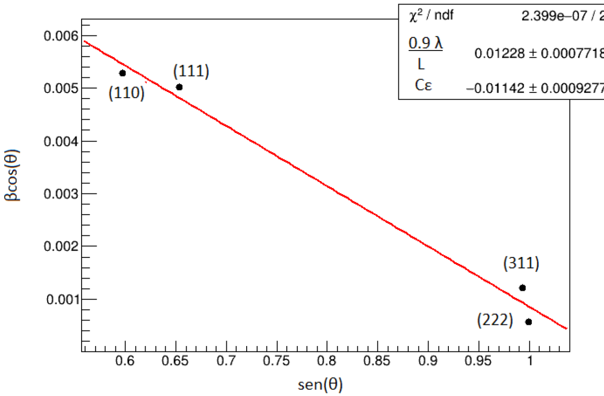

Fig. 5. Williamson-Hall plot for the IrAu film sample #111. L is the crystalline size and Cε the strain.

The samples clustered into two sets, grA (#97, #106, #107, #108, #113) and grB (#99, #111, #112, #114), which have the relative Ir(222) line at mean values 88.079° and 88.003°, respectively, and are about 5 standard deviations apart.

In Fig. 4 T_c measurements of the proximitized iridium samples with gold on top [2], [3], [4] are reported, showing that the two sets grA, red dots, and grB, blue triangles, identify two T_c trends vs. the relative thickness of Ir on Au, which saturate at 130 mK and 180 mK, respectively. The right part of the plot shows the bare Ir film T_c. This means that the proximity effect generated by the gold film conforms to the T_c of the bare Iridium film but does not appear to have an effect on the crystal structure, as shown in Fig. 1 and following description.

Since it is known that the peak position and FWHM identify the crystallite size, that is, the dimension of the oriented domain along the direction identified by the considered line. The crystallite size L for the main Ir (111) line was obtained through Scherrer's formula:

$$L = \frac{0.9\ \lambda}{\beta \cos(\theta)}, \tag{1}$$

TABLE II

AVERAGE VALUE L AND RELATED UNCERTAINTY σ(L) OF THE (111) CRYSTAL SIZE FOR SAMPLES BELONGING TO GROUPS GRA AND GRB, WITH CRITICAL TEMPERATURES OF 130 AND 180 MK. VALUES ARE CALCULATED BY MEANS OF THE SCHERRER FORMULA FROM THE DATA IN TABLE I

T_c	L (111) [nm]	$\sigma(L)$ [nm]
grA 130 mK	25.0	1.5
grB 180 mK	32.9	0.7

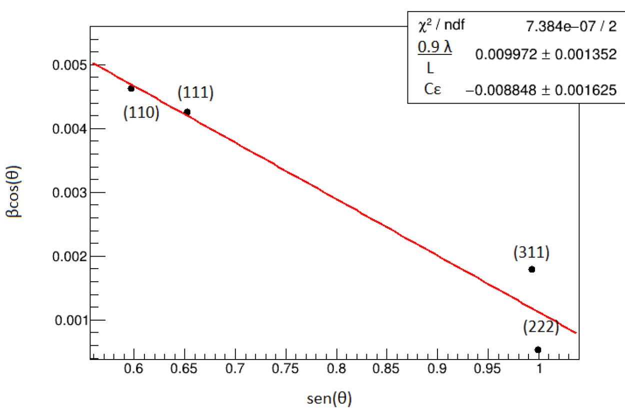

Fig. 6. Williamson-Hall plot for the IrAu film sample #108. L is the crystalline size and Cε the strain.

TABLE III

CRYSTALLINE SIZE L FROM THE WILLIAMSON-HALL MODEL OF THE TWO SAMPLES CONSIDERED AND THE AVERAGE VALUE OF THE TWO GROUPS OF SAMPLES AT TC OF 130 AND 180 MK, RESPECTIVELY

Sample	L [nm]
#108 130 mK	10.6
#111 180 mK	13.9
grA 130 mK	9.1
grB 180 mK	12.7

where $\lambda = 0.15046$ nm is the wavelength of Cu-Kα source, θ is the diffraction peak angle and β the FWHM of peak. It is found that the samples cluster around two average values given in Table II.

The values found in Table II are not completely consistent with literature for PLD depositions without substrate heating [7], [8], but appear more similar to those observed with a PLD deposition with substrate heated to 500 °C. Therefore, we assumed that non-uniform strain in the Ir film structure can contribute to the lattice deformation. We performed an analysis according to Williamson-Hall model [9], which also takes strain into account, on samples #108 and #111, in which lines (311) are also visible. Figs. 5 and 6 show the Williamson-Hall plots for the two samples examined. From these we were able to calculate the crystal size of the whole structure by finding values consistent with PLD deposition of Ir without substrate heating, as shown in Table III, along with the average values of the two groups of samples, gr130 and gr180.

IV. Conclusion and Perspectives

We observe evidence of two sample populations based on Ir films on Si (100) that cluster around two values of T_c, 130 and 180 mK, respectively. Structural analyses with XRD show a correlation between crystal size and T_c that are reproducible with different analyses, Scherrer and Williamson-Hall, where a larger grain size is related to a higher critical temperature. The absolute values depend on the model used, without or with strain, which suggests investigating lattice stress that should play a non-negligible role. We would therefore like to investigate this further with specific measurements on the effect of lattice stress. It should also be noted that the presence of Au in bilayer films does not seem to produce any effect on structure and appears sub-dominated. The Au film has the sole effect of decreasing T_c by proximity effect [10].

Acknowledgment

The authors would like to thank M. Rigano of the University of Genova, L. Parodi, A. Bevilacqua, F. Siccardi of INFN of Genova for the technical support.

References

[1] M. D'Andrea et al., "ATHENA X-IFU demonstration model: First joint operation of the main TES array and its Cryogenic AntiCoincidence detector (CryoAC)," *J. Low Temp. Phys.*, vol. 209, no. 3/4, pp. 433–440, 2022, doi: 10.1007/s10909-022-02786-w.

[2] C. Macculi et al., "The Cryogenic AntiCoincidence detector for ATHENA X-IFU: The project status," *J. Low Temp. Phys.*, vol. 199, pp. 416–424, 2020.

[3] M. Biasotti et al., "The phonon-mediated TES cosmic ray detector for focal plane of ATHENA X-ray telescope," *J. Low Temp. Phys.*, vol. 199, pp. 225–230, 2020, doi: 10.1007/s10909-020-02348-y.

[4] M. D'Andrea et al., "The demonstration model of the ATHENA X-IFU Cryogenic AntiCoincidence detector," *J. Low Temp. Phys.*, vol. 199, pp. 65–72, 2020, doi: 10.1007/s10909-019-02300-9.

[5] L. F. Barusso et al., "First configurational study of the CryoAC detector silicon chip of the athena X-Ray observatory," *IEEE Trans. Appl. Supercond.*, vol. 33, no. 1, Jan. 2023, Art. no. 2100207, doi: 10.1109/TASC.2022.3222959.

[6] D. Barret et al., "The Athena X-ray Integral Field Unit: A consolidated design for the system requirement review of the preliminary definition phase," *Exp. Astron.*, pp. 1–54, 2023, doi: 10.1007/s10686-022-09880-7.

[7] M. A. El Khakani et al., "Effect of the deposition temperature on the properties of Ir thin films grown by means of PLD," *J. Mater. Res.*, vol. 14, no. 8, pp. 3241–3246, Aug. 1999, doi: 10.1557/JMR.1999.0438.

[8] Y. Gong et al., "Low-temperature deposition of iridium thin films by pulsed laser deposition," *Vacuum*, vol. 82, pp. 594–598, 2008, doi: 10.1016/j.vacuum.2007.09.003.

[9] D. Nath et al., "X-ray diffraction analysis by Williamson-Hall, Halder-Wagner and size-strain plot methods of CdSe nanoparticles-A comparative study," *Mater. Chem. Phys.*, vol. 239, 2020, Art. no. 122021, doi: 10.1016/j.matchemphys.2019.122021.

[10] U. Nagel et al., "Proximity effect in iridium-gold bilayers," *J. Appl. Phys.*, vol. 76, 1994, Art. no. 4262, doi: 10.1063/1.357310.

Open Access provided by 'Università degli Studi di Genova' within the CRUI CARE Agreement